Electronic properties of the graphene/6H-SiC(000$\bar{1}$) interface: A first-principles study

Thushari Jayasekera,[1,*] Shu Xu,[1] K. W. Kim,[2] and M. Buongiorno Nardelli[1,3]
[1]*Department of Physics, North Carolina State University, Raleigh, North Carolina 27695-8202, USA*
[2]*Department of Electrical and Computer Engineering, North Carolina State University, Raleigh, North Carolina 27695-7911, USA*
[3]*Computer Science and Mathematics Division, Oak Ridge National Laboratory, Oak Ridge, Tennessee 37831, USA*
(Received 3 February 2011; revised manuscript received 21 April 2011; published 27 July 2011)

Using calculations from first principles, we show how the structural and electronic properties of epitaxial graphene on 6H-SiC(000$\bar{1}$) are determined by the geometry and the chemical functionalization of the interface region. We also demonstrate that these properties can be correctly captured only if a proper treatment of the van der Waals interactions is included in the theoretical description based on density functional theory. Our results reproduce the experimentally observed *n*-type doping of monolayer epitaxial graphene and prove the possibility of opening a sizable (150 meV) energy gap in the bilayer case under special growth conditions. Depending on the details of the bonding at the interface, we are able to interpret recent experimental observations and provide a clear insight into the mechanisms of charge transfer and interface stability.

DOI: 10.1103/PhysRevB.84.035442 PACS number(s): 73.22.Pr, 61.48.Gh, 71.15.Mb, 81.05.ue

I. INTRODUCTION

Although epitaxial graphene was first synthesized in 1975,[1] the first demonstration of its use in lithographically patterned devices in 2004[2] dramatically revamped the interest in this material and has paved the way to potential new classes of applications for innovative nanoelectronics.[3,4] Advances in the understanding of epitaxial growth of graphene on SiC, which is the substrate of choice for microchip design, have the potential to revolutionize the semiconductor road map for future decades.[5,6]

Epitaxial graphene on SiC is obtained by the sublimation of Si atoms either from the (0001) surface (Si-face) or from the (000$\bar{1}$) surface (C-face) of 6H- or 4H-SiC polytypes. Si sublimation is achieved by annealing the SiC sample in ultrahigh vacuum (UHV) conditions or at moderate vacuum conditions in the presence of a background gas such as Ar.[7,8]

The growth of epitaxial graphene on the Si-terminated face (0001) is characterized by the presence of an intermediate carbon layer (the "buffer layer") that screens most of the effect of the substrate.[9–11] On the C-terminated face, the situation can be quite different depending on the conditions of growth: Hass *et al*.[12,13] have reported a strongly interacting first C-layer, i.e., a buffer layer on C-face, which is similar to the observation made on the graphene/SiC(0001) interface. On the other hand, a weakly bound or decoupled graphene layer is reported by many other groups.[14–16] Moreover, different growth conditions can lead to different graphitic stacking sequences in multilayered samples: AA,[15] AB,[17] and, most frequently, misoriented (turbostratic)[18] layers have been observed. Such structural differences are paralleled by an equally broad spread in the electronic structure characteristics: de Heer *et al*. reported that C-face epitaxial graphene is *n*-doped with the Dirac point approximately 300 meV below the Fermi level,[7] while Emtsev *et al*. reported this value to be 200 meV.[19,20] *p*-doped epitaxial graphene on the C-face has also been reported.[21–23] Although some of these observations might be biased by uncontrollable ambient conditions, a deeper understanding of the interplay between structure and properties of the graphene/SiC(000$\bar{1}$) interface is of paramount importance.

While the electronic and structural properties of the graphene/SiC(0001) interface have been the subject of many theoretical investigations,[9,11] very few studies have been devoted to the understanding of the properties of the graphene/SiC(000$\bar{1}$) system[10,24] and the results are not always in agreement with the available experimental observations. Here, we use calculations from first principles based on density functional theory (DFT) to study the graphene on SiC(000$\bar{1}$) surface. One common limitation of the DFT calculations is the inability to describe the long-range van der Waals (vdW) forces, which is an essential component of the interaction in layered systems. In this paper, we demonstrate that only by taking vdW interactions into account, one can correctly describe not only the geometry, but also the electronic structure of epitaxial graphene on the SiC(000$\bar{1}$) surface.

The paper is organized as follows. In Sec. II, we discuss the geometry of the interface and give the technical details of our calculations; in Sec. III A, we discuss the importance of the inclusion of dispersion forces in determining correctly the electronic and structural properties of the graphene/SiC system; in Sec. III B, we elaborate on the structural and electronic modifications induced by a change in the interfacial chemistry; and in Sec. III C, we discuss the case of bilayer graphene. We conclude with some final remarks in Sec. IV.

II. METHODOLOGY

On the Si-terminated surface of SiC, a thermal annealing process results in a $\sqrt{3} \times \sqrt{3}R\cos(30^\circ)$ ($R3$) surface reconstruction followed by a $6\sqrt{3} \times 6\sqrt{3}R\cos(30^\circ)$ ($6R3$) reconstruction. Since the periodic unit cell for the $6R3$ structure is large and computationally expensive to simulate, the $R3$ model has been used for most calculations irrespective of the residual 7% mismatch between the $R3$ cell of SiC and the 2×2 cell of graphene. This model correctly reproduces the experimental observations for graphene on SiC(0001), such as the presence of a strongly bonded buffer layer and an electron-doped first graphene layer.[9,11] Even though the $R3$ model is compatible with the C-face termination of SiC, it does not seem to correctly reproduce the experimentally observed

 ©2011 American Physical Society

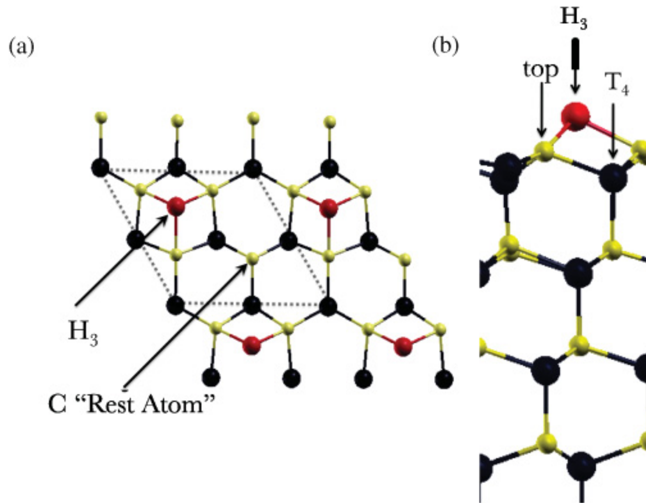

FIG. 1. (Color online) (a) Top view and (b) side view of the $(2 \times 2)_C$ reconstructed model for the SiC(000$\bar{1}$) surface with a Si adatom in the *H3* position. (b) shows all three possible high-symmetry positions *T4*, *H3*, and *top* for the Si adatom. Red (darker gray) atoms are Si adatoms, black atoms are Si in SiC bulk, and yellow (light gray) atoms are C in SiC bulk. The $(2 \times 2)_C$ unit cell is depicted by the dashed lines in the top view (a).

reconstructed structures either for the geometry or for their electronic properties.[10] STM data show that the sublimation on the C-face starts with a 3×3 surface reconstruction, which later evolves into a $(2 \times 2)_C$ reconstruction.[14] In order to follow the experimental observation, we have adapted the atomistic model proposed by Seubert *et al.*[25] and later used by Magaud *et al.*[24] for investigating the C-face epitaxial graphene. In the $(2 \times 2)_C$ reconstructed model proposed by Seubert *et al.*, three out of the four surface C atoms are bonded to a Si adatom. There are three high-symmetry positions that a Si adatom can bind to the C atoms on the open surface [Fig. 1(b)]: *H3*, the threefold coordinated hollow site; *T4*, a position directly on top of a Si atom in the layer underneath; and *top*, an adatom directly binds to a single C atom on the open surface. The *top* position only saturates one dangling bond, and it is clearly unfavorable. Between *H3* and *T4*, *H3* is found to be energetically more stable. In the *H3* adatom configuration, there are still two unsaturated dangling bonds, one on the Si adatom and the other on the unbound C atom, "*the rest atom*" (see Fig. 1). On the reconstructed SiC(000$\bar{1}$) surface, the difference in electronegativity between Si and C induces a charge transfer from the Si adatom to the C rest atom, which is responsible for the surface states observed in the band structure of the combined graphene/SiC system and the pinning of the Fermi energy at the interface [see Sec. III B and Fig. 4(a) for a more detailed discussion]. To minimize residual strain due to lattice mismatch between graphene and the SiC surface, a 5×5 graphene cell is overlaid on a 4×4 SiC cell with $(2 \times 2)_C$ surface reconstruction. This geometry reduces the lattice strain to less than $\sim$1%.

All the calculations are performed in the framework of DFT as it is implemented in the quantum-ESPRESSO package.[26] We have used a $3 \times 3 \times 1$ Monkhorsk-Pack grid for Brillouin zone integration, 20–24 Å vacuum region to separate the slabs, and the geometries have been optimized to forces less than 0.025 eV/Å. In our choice of exchange and correlation functionals, we used both the local density approximation (LDA) (with 65 Ry energy cutoff for the plane-wave expansion) and the generalized gradient approximation (GGA) in the Perdew-Burke-Ernzerhof (PBE) form (40 Ry energy cutoff).[27] It is well known that local or semilocal approximations for the exchange and correlation energy (either LDA or GGA) in DFT fail to account for vdW interactions completely and that the quantitative agreement that one sometimes finds in the description of the bonding in layered systems (such as in graphite) using LDA is due to a fortuitous cancellation of errors that can not be taken as systematically correct for any graphene-based systems. We have included vdW interactions in our calculations for the GGA exchange and correlation functional using an empirical potential of the form $C_6 R^{-6}$ added to the regular density functional energy [GGA(D)] as proposed by Grimme *et al.*[28] and recently implemented by Barone *et al.*[29] in the quantum-ESPRESSO code. Magaud *et al.* have investigated the properties of the C-face epitaxial graphene with the same model within GGA approximation, with no vdW interactions.[24] In this paper, we demonstrate the importance of vdW interactions in these loosely bound layered systems.

III. RESULTS AND DISCUSSION

A. Effect of long-range dispersion forces on the geometry and the electronic structure of the interface

In order to quantify the effect of the inclusion of vdW forces on the interface structure and electronic characteristics, we optimized the geometry of the graphene/SiC system using LDA, GGA, and GGA(D). Table I summarizes the geometrical parameters of the optimized geometries in the three cases, while the corresponding electronic bands are presented in Fig. 2. In GGA, the average distance between the Si adatom and the graphene layer is $\sim$3.29 Å, whereas this distance is 2.64 Å in LDA and 2.61 Å in GGA(D). LDA and GGA(D) give remarkably similar results, an indication that the cancellation of errors in LDA is indeed reproducing the more accurate GGA(D) results. The same similarity is observed in the electronic band structure [shown in Figs. 2(a) and 2(c)]. Both LDA and GGA(D) produce an electron-doped graphene layer with the Dirac point lying $\sim$0.35 eV below the Fermi level. In contrast, GGA results in a neutral graphene layer [Fig. 2(b)] that is in agreement with previous calculations.[24] The ripples in the C layer (reported in Table I) are not strong enough to destroy the π orbital network in the graphene layer in any of the three systems.

TABLE I. Comparison of the geometries (average vertical distance between the Si adatom and the graphene layer d_{average} and the resultant ripple width) with different exchange and correlation (XC) functionals for LDA, GGA, and GGA(D).

XC functional	d_{average}	Ripple width
LDA	2.64 Å	0.16 Å
GGA	3.29 Å	0.04 Å
GGA(D)	2.61 Å	0.27 Å

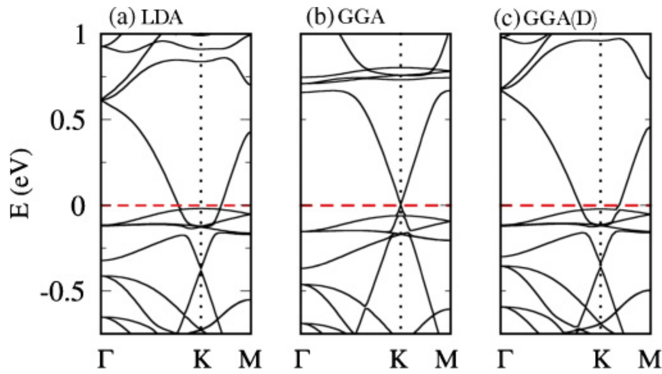

FIG. 2. (Color online) The electronic band structures (along ΓKM path) of epitaxial graphene on the C face of SiC in the Si adatom surface reconstructed model, calculated with (a) LDA, (b) GGA, and (c) GGA(D). Fermi level is set to 0 eV.

According to the results shown in Fig. 2(c), there is no evidence for the presence of a strongly bound layer or a buffer layer. In fact, the first C layer on the $(000\bar{1})$ surface shows graphenic properties in contrast to the buffer layer on the Si face, and epitaxial graphene on SiC$(000\bar{1})$ is electron doped as the experiments suggested. The n-doped behavior is hidden when the vdW interactions are not included in the calculation.[24] The electronic bands near the Fermi level are identified as dangling bond states of the C rest atoms [see Fig. 4(a)]. Si adatom dangling bond states are empty and lie around 1 eV above the Fermi level.

B. Effect of interfacial chemistry

The existence of dangling bond states at the interface suggests the possibility of passivation induced by external chemical species during the growth process. We have considered two prototypical cases: a *half-passivated* and a *fully passivated* interface. Only the C rest atoms are passivated in the *half-passivated* interface, leaving a dangling bond on the Si adatoms. The C rest atom–passivated system is 4.9 meV (per C atom in the graphene layer) more favorable than the Si-adatom–passivated system. Both the Si adatoms and the C rest atoms are passivated with H in the *fully passivated* system. The differences among the three configurations are striking: In the unpassivated interface, the graphene layer maintains its individuality although it becomes n-doped; in the half-passivated system, the graphene-Si adatom interaction is so strong that the graphene binds strongly with the substrate, giving rise to a buffer layer similar to what happens for the growth on the Si-terminated face; finally, the fully passivated system shows a completely decoupled graphene layer with the ideal Dirac band dispersion.

TABLE II. Comparison of the geometries (the average vertical distance d_{average}, between the Si adatom and the graphene layer and the resultant ripple width) for different interfacial configurations.

System	d_{average}	Ripple width
Unpassivated	2.61Å	0.27 Å
Half-passivated	2.28 Å	0.50 Å
Full passivated	3.83 Å	0.10 Å

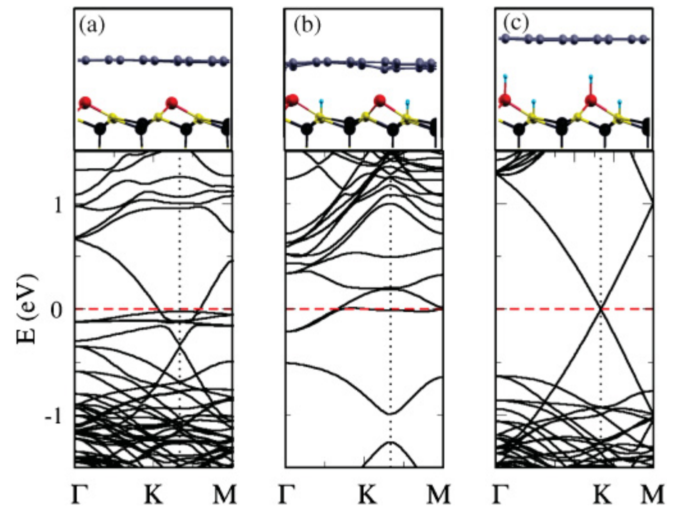

FIG. 3. (Color online) The electronic band structures (along ΓKM path) of graphene on the C face of SiC with different interfacial passivation: (a) unpassivated, (b) half-passivated, and (c) fully passivated. The upper panel shows the atomic configuration of the three interface configurations. Fermi level is set to 0 eV.

Our results are summarized in Fig. 3, and the parameters describing the three optimized geometries are tabulated in Table II. In the half-passivated case, the passivation of the C rest atom prevents the Si-C charge transfer that occurs in the unpassivated interface. Thus, the Si dangling bond states become half-occupied and interact strongly with the C atoms of the graphene layers. The average distance between the Si adatoms and the graphene layer shortens considerably, ∼2.28 Å, and the graphene layer shows a higher degree of vertical deformation with an average ripple width of 0.5 Å. Since the graphene layer now lies closer to the substrate, the interaction between the Si adatoms and the C atoms disrupts the sp^2 hybridization of the π orbital network and the linear band dispersion at the Dirac point [Fig. 4(b)]. Once the interface is fully passivated with H, the graphene layer effectively decouples from the substrate with a separation of 3.8 Å (with a negligible 0.1 Å ripple width), and therefore shows neutral graphene characteristics as shown in Fig. 4(c).

These results can, in part, explain the wide range of variation of the electronic properties observed during growth of graphene on the C-face. In particular, depending on the

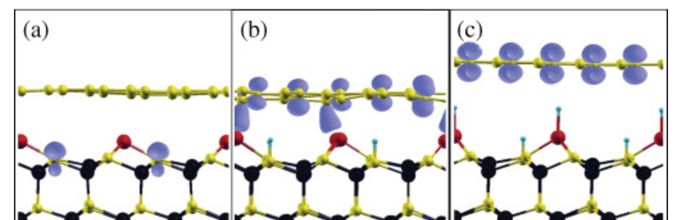

FIG. 4. (Color online) The electron density of the states localized on the interface at the Dirac point for (a) unpassivated, (b) half-passivated, and (c) fully passivated systems. Blue isosurfaces correspond to 0.15×10^{-3} electrons.

TABLE III. Vertical distance between the first graphene layer and the Si adatoms Δ_0 and between the first and second C layers Δ_1 for different passivations and stacking sequences.

System	Δ_0	Δ_1
Unpassivated (AA)	2.62 Å	3.47 Å
Unpassivated (AB)	2.60 Å	3.23Å
Half-Passivated (AA)	2.26 Å	3.41 Å
Half-Passivated (AB)	2.27 Å	3.25 Å
Full Passivated (AA)	3.86 Å	3.46 Å
Full Passivated (AB)	3.86 Å	3.24 Å

experimental conditions, passivation might occur and give rise to samples that can, in turn, be neutral or n-doped, and with a geometry that can vary between fully decoupled or completely distorted by interface bonds (buffer layer).

C. Bilayer graphene on SiC(000$\bar{1}$)

The effect of the inclusion of vdW forces in the calculations is even more pronounced in the case of bilayer graphene, where the intralayer interactions of the two graphene planes add to the stability of the interface. When more than one layer of graphene is grown on SiC(000$\bar{1}$), the stacking of the layers can also vary depending on the growth conditions: the observation of islands of Bernal stacking (AB),[17] AA stacking,[15] and of distorted (turbostratic)[18] sequences have been reported in the literature. While it is important to investigate the properties of turbostratic stacking sequences,[31,32] in this paper we focus on the comparison between AA and AB geometries. Only little has been done on the theoretical side on more than one C layer on the SiC(000$\bar{1}$) surface, and indeed we are aware of only few studies where different hexagonal stacking sequences have been characterized on the unrealistic $R3$ reconstruction.[10,15] Table III compares the interlayer distance Δ_1 and the Si adatom/first-C-layer distance Δ_0 for various interface configurations. Similar to the monolayer case, the shortest Si adatom-graphene distance and the higher ripple width are found in the half-passivated system, where the strong interaction between the Si dangling bond state and the first graphene layer determine the geometrical structure.

Of course, different geometries induce different electronic behaviors. In Fig. 5, we display the calculated energy bands for unpassivated [(a) AB stacking, (b) AA stacking], half-passivated [(c) AB stacking, (d) AA stacking], and fully passivated [(e) AB stacking, (f) AA stacking] interfaces and we analyze the effect of the layer ordering on the electronic properties of the systems. In both the unpassivated and fully passivated cases, we observe a marked distinction between the AB and AA stacking, although the difference in their relative stability is negligible (in all configurations, the AB stacking is energetically slightly more favorable by a few meV/C atom).

In the ideal suspended graphene geometry, the AB stacking causes a symmetry breaking that induces an inequivalence of the C atoms in the benzene rings. This inequivalence is responsible for the opening of a small energy gap. On the other hand, in the AA stacking sequence, this symmetry breaking does not take place and the two graphene planes are effectively independent and display a typical double Dirac cone structure.[30]

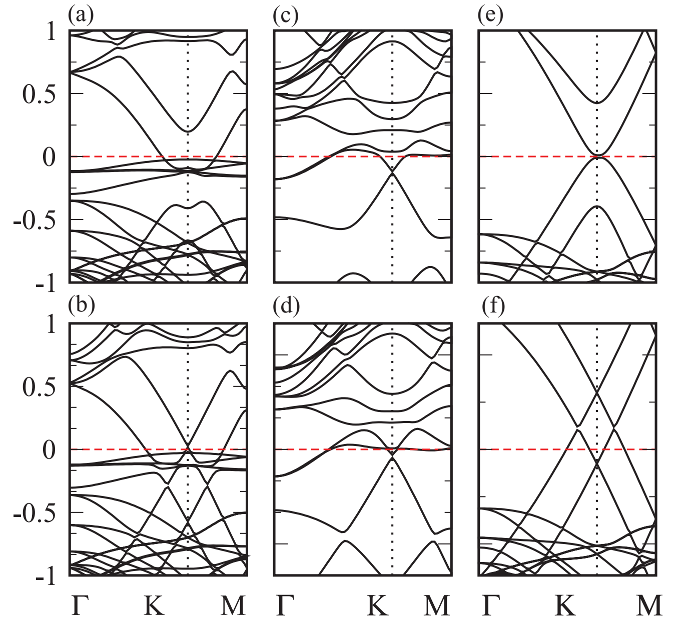

FIG. 5. (Color online) Electronic band structures (along ΓKM path) of graphene bilayers on the $(2 \times 2)_c$ SiC(000$\bar{1}$) surface with (a), (b) unpassivated, (c), (d) half-passivated, and (e), (f) full-passivated interface. The upper [(a), (c), (e)] and lower [(b), (d), (f)] panels show the electronic bands for AB and AA stackings, respectively.

When grown epitaxially on SiC(000$\bar{1}$), the bilayer maintains some of its ideal characteristics. This is better observed in the case of the fully passivated interface, where the degree of decoupling between the bilayer and the substrate makes the system behave almost as in the ideal case. The AB geometry [Fig. 5(e)] displays a small energy gap (of the order of a few meV), while the AA system [Fig. 5(f)] shows evidence of the double Dirac cone structure. It is important to note, though, that the Fermi energy is lower than the Dirac point energy, so that the bilayer is effectively p-doped.

The situation changes drastically in the unpassivated case: The AB bilayer [Fig. 5(a)] electronic structure displays a large ($\sim$150 meV) energy gap that is induced by the fact that the first graphene layers screen only partially the effect of the substrate on the second layer, thus, enhancing the intralayer interaction and the symmetry breaking between the two inequivalent Dirac points of the two layers. The system is still n type with the Fermi level pinned by the C rest atom interface states. On the contrary, in the AA stacking sequence [Fig. 5(b)], the electronic bands show a higher degree of decoupling and display the typical double crossing of the Dirac cones, with only a negligible band-gap opening. Finally, in the half-passivated system [Figs. 5(c) and 5(d)], the top layer behaves effectively as a single graphene layer on a C buffer, a situation that reminds again of the Si-face growth geometry. In both layer orderings, the graphene is n type.

IV. CONCLUSIONS

In summary, we have investigated the properties of epitaxial graphene on SiC(000$\bar{1}$) surface with the Si adatom reconstructed model of Seubert *et al*. and we have demonstrated

the importance of the inclusion of van der Waals interactions in determining the correct equilibrium geometries and their electronic properties. Our analysis of interfacial chemistry and passivation of the interface shows how the *n*-type behavior of the system and the relative band alignment between SiC and graphene can be varied, and provides an insight into the reason why experimental observations can give different results depending on the sample growth or other environmental conditions.[33]

ACKNOWLEDGMENTS

This work was supported, in part, by the DARPA/HRL CERA, the FCRP FENA programs, and NSF. M.B.N. wishes to acknowledge partial support from the Office of Basic Energy Sciences, US Department of Energy at Oak Ridge National Laboratory, under Contract No. DE-AC05-00OR22725 with UT-Battelle, LLC. Calculations have been performed at NCCS-ORNL and HPC-NCSU.

*thusharij@gmail.com

[1] A. J. VanBommel, J. E. Crombeen, and A. VanTooren, Surf. Sci. **48**, 463 (1975).
[2] C. Berger, Z. Song, T. Li, X. Li, A. Y. Ogbazghi, R. Feng, Z. Dai, A. N. Marchenkov, E. H. Conrad, P. N. Fiirst, and W. A. de Heer, J. Phys. Chem. B **108**, 19912 (2004).
[3] K. S. Novoselov, A. K. Geim, S. V. Morozov, D. Jiang, Y. Zhang, S. V. Dubonos, I. V. Grigorieva, and A. A. Firsov, Science **306**, 666 (2004).
[4] Y. Zhang, Y. W. Tan, H. L. Stormer, and P. Kim, Nature (London) **438**, 201 (2005).
[5] W. A. de Heer, C. Berger, X. Wu, P. N. First, E. H. Conrad, X. Li, T. Li, M. Sprinkle, J. Hass, M. L. Sadowski, M. Potemski, and G. Martinez, Solid State Commun. **143**, 92 (2007).
[6] K. S. Novoselov, A. K. Geim, S. V. Morozov, D. Jiang, M. I. Katsnelson, I. V. Grigorieva, S. V. Dubonos, and A. A. Firsov, Nature (London) **438**, 197 (2005).
[7] W. A. de Heer, C. Berger, X. Wu, M. Sprinkle, Y. Hu, M. Ruan, J. A. Storscio, P. N. First, R. Haddon, B. Piot, C. Faugeras, M. Potemski, and J. S. Moon, J. Phys. D: Appl. Phys. **43**, 374007 (2010).
[8] Luxmi, N. Srivastava, G. He, R. M. Feenstra, and P. J. Fisher, Phys. Rev. B **82**, 235406 (2010).
[9] A. Mattausch and O. Pankratov, Phys. Rev. Lett. **99**, 076802 (2007).
[10] F. Varchon, R. Feng, J. Hass, X. Li, B. N. Nguyen, C. Naud, P. Mallet, J. Y. Veuillen, C. Berger, E. H. Conrad, and L. Magaud, Phys. Rev. Lett. **99**, 126805 (2007).
[11] T. Jayasekera, B. D. Kong, K. W. Kim, and M. Buongiorno Nardelli, Phys. Rev. Lett. **104**, 146801 (2010).
[12] J. Hass, W. A. de Heer, and E. H. Conrad, J. Phys. Condens. Matter **20**, 323202 (2008).
[13] C. Berger, X. Wu, P. N. First, E. H. Conrad, X. Li, M. Sprinkle, J. Hass, F. Varchon, L. Magaud, M. Sadowski, M. Potemski, G. Martinez, and W. A. de Heer, Adv. Solid State Phys. **47**, 145 (2008).
[14] F. Hiebel, P. Mallet, F. Varchon, L. Magaud, and J. Y. Veuillen, Phys. Rev. B **78**, 153412 (2008).
[15] J. Borysiuk, K. Soltys, and J. Piechota, e-print arXiv:1006.1040.
[16] M. Sprinkle, D. Siegel, Y. Hu, J. Hicks, A. Tejeda, A. Taleb Ibrahimi, P. LeFevre, F. Bertran, S. Vizzini, H. Enriquez, S. Chiang, P. Soukiassian, C. Berger, W. A. de Heer, A. Lanzara, and E. H. Conrad, Phys. Rev. Lett. **103**, 226803 (2009).
[17] M. Orlita, C. Faugeras, J. Borysiuk, J. M. Baranowski, W. Strupiński, M. Sprinkle, C. Berger, W. A. de Heer, D. M. Basko, G. Martinez, and M. Potemski, Phys. Rev. B **83**, 125302 (2011).
[18] J. Hass, F. Varchon, J. E. Millán-Otoya, M. Sprinkle, N. Sharma, W. A. de Heer, C. Berger, P. N. First, L. Magaud, and E. H. Conrad, Phys. Rev. Lett. **100**, 125504 (2008).
[19] K. V. Emtsev, F. Speck, Th. Seyller, L. Ley, and J. D. Riley, Phys. Rev. B **77**, 155303 (2008).
[20] C. Berger, Z. Song, X. Li, X. Wu, N. Brown, C. Naud, D. Mayou, T. Li, J. Hass, A. N. Marchenkov, E. H. Conrad, P. N. First, and W. A. de Heer, Science **312**, 1191 (2006).
[21] Y. M. Lin, C. Dimitrakopoulos, D. B. Farmer, S. J. Han, Y. Q. Wu, W. J. Zhu, D. K. Gaskill, J. L. Tedesco, R. L. Myerd-Ward, C. R. Eddy Jr., A. Grill, and P. Avouris, Appl. Phys. Lett. **97**, 112107 (2010).
[22] D. L. Miller, K. D. Kubista, G. M. Rutter, M. Ruan, W. A. de Heer, P. N. First, and J. A. Stroscio, Science **324**, 924 (2009).
[23] T. Hofmann, A. Boosalis, B. Kuhne, C. M. Herzinger, J. A. Woollam, D. K. Gaskill, J. L. Tedesco, and M. Schubert, Appl. Phys. Lett. **98**, 041906 (2011).
[24] L. Magaud, F. Hiebel, F. Varchon, P. Mallet, and J. Y. Veuillen, Phys. Rev. B **79**, 161405 (2009).
[25] A. Seubert, J. Bernhardt, M. Nerding, U. Starke, and K. Heinz, Surf. Sci. **45**, 454 (2000).
[26] Paolo Giannozzi *et al.*, J. Phys. Condens. Matter **21**, 395502 (2009).
[27] For GGA, we used C.pbe-rrkjus.UPF, H.pbe-rrkjus.UPF, and Si.pbe-n-van.UPF pseudopotentials for C, H, and Si, respectively. For LDA, C.pz-vbc.UPF, H.pz-vbc.UPF, and Si.pz-vbc.UPF pseudopotentials were used.
[28] S. Grimme, J. Comput. Chem. **25**, 1463 (2004).
[29] V. Barone, M. Casarin, D. Forrer, M. Pavone, M. Sambi, and A. Vittadini, J. Comput. Chem. **30**, 934 (2009).
[30] E. J. Mele, Phys. Rev. B **81**, 161405 (2010).
[31] O. Pankratov, S. Hensel, and M. Bockstedte, Phys. Rev. B **82**, 121416 (2010).
[32] M. Chen, W. Sun, G-C. Guo, and L. He, Phys. Status Solidi B **248**, 1690 (2011).
[33] A. N. Sidorov *et al.* (unpublished).